Materials Science & Engineering C 114 (2020) 111034

Contents lists available at ScienceDirect

Materials Science & Engineering C

journal homepage: www.elsevier.com/locate/msec

Intrinsic peroxidase-like activity of graphene nanoribbons for label-free colorimetric detection of dopamine

Simindokht Rostami[a], Ali Mehdinia[b,*], Ali Jabbari[a]

[a] Department of Analytical Chemistry, Faculty of Chemistry, K. N. Toosi University of Technology, Tehran, Iran
[b] Department of Marine Living Science, Ocean Sciences Research Center, Iranian National Institute for Oceanography and Atmospheric Science, Tehran, Iran

ARTICLE INFO

Keywords:
Graphene nanoribbons
Peroxidase-like activity
Nanozyme
Colorimetric detection
Dopamine

ABSTRACT

Graphene nanoribbons (GNR) with intrinsic peroxidase mimic activity were introduced as a nanozyme with catalytic activity in oxidation of a typical chromogenic peroxidase substrate, 3,3′,5,5′-tetramethylbenzidine (TMB), in the presence of H_2O_2. The proposed artificial enzyme was used as a label-free biosensor for rapid and sensitive colorimetric detection of dopamine (DA) according to a blue color fading which occurred due to the inhibition of TMB oxidation. Attractively, GNR exhibited an excellent catalytic activity over other carbon-based nanostructures due to its unique and extraordinary structural properties. Considering the changes of A_{653} versus DA concentration, a good linear dependency was achieved in the concentration range of 0.1–50 μM (0.1–1 and 2.5–50 μM) with a detection limit of 0.035 μM. The present peroxidase mimetic as a simple and rapid label-free sensor was successfully applied for detection of DA in serum samples, suggesting a promising sensitive sensing platform with great potential for biological and diagnostic applications.

1. Introduction

In recent years there has been growing interest in developing simple and cost-effective nanosensors for rapid detection of biomolecules and biomarkers [1,2]. Nanomaterials with intrinsic peroxidase-like activity (nanozymes) have been emerged as a new generation of artificial enzymes [3–5]. Nowadays, these artificial enzymes are widely used as favorable alternatives to natural enzymes owing to their tunable and fascinating catalytic activity, high stability, long-term storage, simple preparation, robustness to harsh conditions and low cost [6,7]. As it has been widely investigated, the studied nanomaterial-based enzyme mimics have shown great potential to effectively overcome the intrinsic drawbacks of native enzymes such as tedious and high-cost purification and preparation steps, poor stability, extremely sensitive catalytic performance towards environmental conditions, limited storage and availability which have enormously restricted their practical applications [6]. The enzyme mimics have received widespread attention in different application fields including (bio)sensing, immunoassay, imaging, disease diagnosis, cancer therapy and environmental monitoring [3–6,8–10]. Over the last few years, various nanomaterials including noble metal nanoparticle, metal oxide nanoparticle, carbon-based nanostructures and numerous nanocomposites and nanohybrids have been exhibited efficient enzyme-like activity for detection of different analytes [11–13]. Among the large variety of these nanozymes, carbon-based nanomaterials including carbon dot [14–18], carbon nanotube [19–21], graphene dot [22–24], graphene oxide [19,25–28] and their derivatives [10,29,30] have gained considerable research interest as a significant branch of artificial enzymes and promising colorimetric sensing platforms due to their unique catalytic activities.

Graphene nanoribbons (GNR) are narrow strips of graphene sheets with width < 50 nm and quasi one dimensional (1D) structure in nature. As it is well known, GNR displays fantastic electrocatalytic activity owning to their fascinating physicochemical properties which include large specific surface area, high length-to-width ratio, straight edges, high chemical stability and electrical conductivity, excellent biocompatibility, abundant oxygen-containing functional groups and accessible chemically active sites [31–33]. Additionally, GNR possesses more open-ended structures, rich edge defects and high edge density which discriminate it from all other graphene-based nanomaterials [31,34]. As it is generally accepted, in comparison to the basal planes, the electrochemical reactivity of graphene-based nanomaterials at their edge planes is higher than other places by several orders of magnitude [31,35–37]. Therefore, it can be concluded that the fascinating catalytic behavior of GNR originates from its rich edge defects and edge density which results in rapid electron transfer. Consequently, this fact could be responsible for the more favorable electrocatalytic performance of GNR over other graphitic materials. Taking this advantage, GNR is getting a popular and qualified platform in sensing and enzymatic biosensing

* Corresponding author.
E-mail address: mehdinia@inio.ac.ir (A. Mehdinia).

https://doi.org/10.1016/j.msec.2020.111034
Received 20 January 2020; Received in revised form 26 April 2020; Accepted 28 April 2020
Available online 01 May 2020

approaches [32].

Dopamine (DA), as a crucial catecholamine neurotransmitter, plays an important role in the nervous system [38,39]. Abnormal DA concentration can lead to several neurological disorders and diseases including Schizophrenia, Alzheimer's and Parkinson's disease [40,41]. Therefore, selective quantitative detection of DA is essential for disease diagnosis. Hence, many efforts have been made to develop an accurate and sensitive method for detection and determination of DA levels in biological samples. To date, numerous methods including electrochemical analysis [42–50], fluorescence [51,52] and high performance liquid chromatography [53] have been widely applied for detection and determination of DA concentration. However, these accurate traditional methods suffer from some limitations such as complexity, time-consuming and high-cost. Recently, simple colorimetric sensing approaches based on the application of nanozymes have been paid significant attention as promising alternatives to overcome the mentioned shortcomings that enable time and cost effective detection of DA [54].

The present study demonstrates an enhanced intrinsic peroxidase-like activity of GNR over GO and MWCNT. Also, this work describes the application of label-free GNR as a nanozyme for rapid colorimetric detection of DA. As known so far, the functionalization and adequate hybridization of nanomaterials could be an efficient strategy to enhance their catalytic performance due to the synergic effect [55]. Herein, the catalytic activity of GNR was evaluated without any further functionalization/hybridization step to avoid complex, time-consuming and high-cost surface modification steps [56]. Therefore, the catalytic performance of GNR was investigated as a label-free nanozyme. However, hybridization of GNR with other nanostructures would be another promising strategy to introduce a new platform with enhanced catalytic activity and improved sensitivity for future studies particularly when a sensor with high sensitivity is required for detection of very low concentrations. The proposed simple colorimetric sensing approach was established based on the fact that DA can cause a blue color fading and a decrease in the absorption intensity due to its inhibitory effect on the peroxidase mimetic activity of GNR. The observed changes which are attributed to change in DA concentration were satisfactorily employed for detection of DA in human serum sample.

2. Experimental

2.1. Chemicals

Multi-walled carbon nanotubes (MWCNT) were supplied from Sigma-Aldrich (Switzerland). 3,3′,5,5′-Tetramethylbenzidine (TMB) purchased from Sigma-Aldrich (Switzerland), was a kind gift of Pro. Anja Boisen (DTU, Lyngby, Denmark). Graphite powder, potassium permanganate ($KMnO_4$, 99%), sulfuric acid (H_2SO_4, 98%), sodium acetate trihydrate (NaOAC) and hydrogen peroxide (H_2O_2, 30%) were provided from Merck (Darmstadt, Germany). All the used chemicals were of analytical grade and utilized without further purification. All solutions were prepared with deionized water.

2.2. Characterization

The UV–Vis absorption spectra were recorded using the UV–Vis spectrophotometer Unico 4802 (USA) in the wavelength range of 500–800 nm. A Zeiss EM10C-100 KV high-resolution transmission electron microscope and field emission scanning electron microscopy (FESEM) model SIGMA VP (Zeiss, Germany) were applied for characterization of MWCNT and GNR structure. FTIR spectra of the nanostructures were recorded using a Bruker VerTex70 (Bruker, Germany) spectrometer and Raman spectra were obtained by employing a micro Raman spectrometer Avantes (The Netherlands) with a 532 nm Nd-YAG excitation laser source. X-ray diffraction (XRD) pattern of MWCNT, GO and GNR were acquired by the Cu Kα radiation source using the diffractometer (X'Pert PRO MPD PANalytical, the Netherlands) in the range of 5–80° with a step size of 0.02°. The specific surface area of samples was determined using Brunauer-Emmett-Teller (BET) isotherm obtained by a measurement system; model BEISORP Mini (Microtrac BEL Corp, Japan). Prior to BET analysis, the samples were first degassed under vacuum for 12 h at 120 °C.

2.3. Synthesis of graphene nanoribbons (GNR)

GNR was prepared based on the previously reported method with some modifications [57]. Briefly, 250 mg suspended MWCNT in 50 mL of concentrated H_2SO_4 was stirred for 24 h at room temperature. Then, $KMnO_4$ (1.25 g) was added into the mixture, agitated for 1 h at room temperature and after that stirring was continued for another 1 h at 65 °C to guarantee the reaction went to completion. The mixture was allowed to cool down to room temperature. Then it was poured into 250 mL cool water containing 25 mL H_2O_2 solution (30%) in an ice bath. This solution was centrifuged and the residue was washed several times with 20% HCl and deionized water. The final product was washed with ethanol and dried at 60 °C in the oven. Graphene oxide (GO) was prepared according to the improved Hummers' method [58].

2.4. Peroxidase-like activity of GNR

Peroxidase-like activity of GNR in the presence of H_2O_2 and TMB was evaluated and compared with the catalytic activity of GO and MWCNT. To this aim, 100 μL of each nanostructure solution with concentration of 0.5 mg mL^{-1} was added to 300 μL of NaOAC-HOAC buffer (0.2 M, pH 4). This solution was incubated for 5 min at 35 °C and then 50 μL of freshly prepared H_2O_2 (50 mM) and TMB (5 mM) were added into it. The UV–Vis spectrum of this mixture was recorded using a UV–Vis spectrophotometer immediately after addition of H_2O_2 and TMB. In the steady-state kinetic assay, different concentrations of H_2O_2 and TMB substrates were used for investigation of GNR catalytic activity.

2.5. Colorimetric detection of DA

For detection of DA using GNR as a nanozyme, 50 μL of DA solution with different concentrations (0–1000 μM) and 100 μL GNR solution (0.1 mg mL^{-1}) were added to 250 μL of NaOAC-HOAC buffer (0.2 M, pH 4). The mixture was incubated for 5 min at 35 °C and then 50 μL of H_2O_2 (50 mM) and TMB (2.5 mM) were added to the incubated solution. This mixture was incubated for 10 min at 40 °C. The absorption intensity of the produced ox-TMB was recorded at 653 nm using the UV–Vis spectrophotometer and A_{653} was considered for further quantification of DA concentration.

2.6. Preparation of real sample

For verifying the applicability of the proposed nanozyme, GNR was applied for detection of DA in human serum samples. The serum samples were centrifuged and the supernatant was diluted. Given amounts of DA standard solution were added to the diluted serum sample. The serum samples and also the spiked samples with final concentrations of 0.2, 0.4 and 0.8 μM were evaluated for detection of DA via the enzyme-like activity of GNR as described in Section 2.5.

3. Results and discussion

3.1. Characterization of synthesized GNR

GNR was synthesized through the longitudinal unzipping of MWCNT. Fig. 1 demonstrates the characterization of the prepared GNR and its pristine MWCNT. An optical absorption band located at 245 nm appeared in the UV–Vis spectrum of GNR attributed to π-π* transition of aromatic C—C while the absorption spectrum of the pristine MWCNT

exhibits two peaks at 240 and 256 nm (Fig. 1a). Fig. 1b displays the FTIR spectra of GNR and MWCNT. The appeared absorption bands attributed to the stretching vibration of O—H band situated at 3400 cm^{-1}, C═O at 1714 cm^{-1}, aromatic C═C at 1570 cm^{-1}, epoxy and alkoxy C—O—C bands at 1220 and 1040 cm^{-1}, respectively, confirmed the synthesize and formation of oxygen-containing functionalities on the surface of GNR through chemical oxidation of MWCNT. Fig. 1c illustrates the Raman spectra of MWCNT, GNR and GO. In the Raman spectrum of MWCNT, the peaks positioned on 1337 and 1568 cm^{-1} are attributed to D and G bands, respectively. D band describes the structural disorder and G bands correspond to sp^2 carbon atoms vibration [59]. Compared to MWCNT, a D band with higher intensity can be observed in the Raman spectrum of GNR and GO which indicates the presence of oxidized groups, formation of sp^3 carbon atoms and increasing in disorder and structural defect of GNR and GO structure [59]. Also, the surface defect density and structural disorder can be obtained based on the ratio intensity of D and G bands (I_D/I_G). According to the recorded spectra, I_D/I_G ratios were 0.37, 0.9 and 1.1 for MWCNT, GO and GNR, respectively. The obtained higher I_D/I_G ratio for GNR is another evidence for an increase in edge defect density after longitudinal unzipping of MWCNT, formation of oxygen-containing functionalities with sp^3 hybridized carbon atoms and a decrease in sp^2 carbon atoms. Fig. 1d exhibits the XRD patterns of MWCNT, GNR and GO. As illustrated, two characteristic peaks were observed at 25.9° and 42.88° for MWCNT assigned to crystalline planes of (002) and (100), respectively, while in the XRD pattern of GNR a broad peak appeared at 24.9°. Also, the XRD pattern of GO exhibited a strong peak at 10.5° and a weak peak at 42.8° which are attributed to (002) and (100) planes. Compared to GO, the appeared peak at 24.9° in the diffraction pattern of GNR indicates that oxygen functionalities mainly distribute along the edge of GNR and a few groups on its basal plane [33]. The interlayer spacing (d) of 3.56°A was obtained for GNR whereas it was 3.43°A for MWCNT. Indeed, the interlayer space enlargement in GNR confirms the presence of defects and generation of oxygen-containing functional groups in its structure. The estimated surface area of MWCNT, GO and GNR using BET isotherms were found to be 238, 277 and 410 $m^2\ g^{-1}$, respectively. The TEM images of MWCNT and GNR are illustrated in Fig. 2a and b, respectively. Fig. 2b exhibits the narrow strips of graphene with an approximate width of 35–40 nm which are clearly wider than pristine MWCNT. Also, Fig. S1 shows another TEM image of GNR which can also demonstrate the yield of MWCNT unzipping and GNR production. The FESEM images of MWCNT and GNR are shown in Fig. 2c and d, respectively. According to Fig. 2c, the average size of the synthesized GNR was found to be about 32 nm. These obtained founding confirm the MWCNT longitudinal opening.

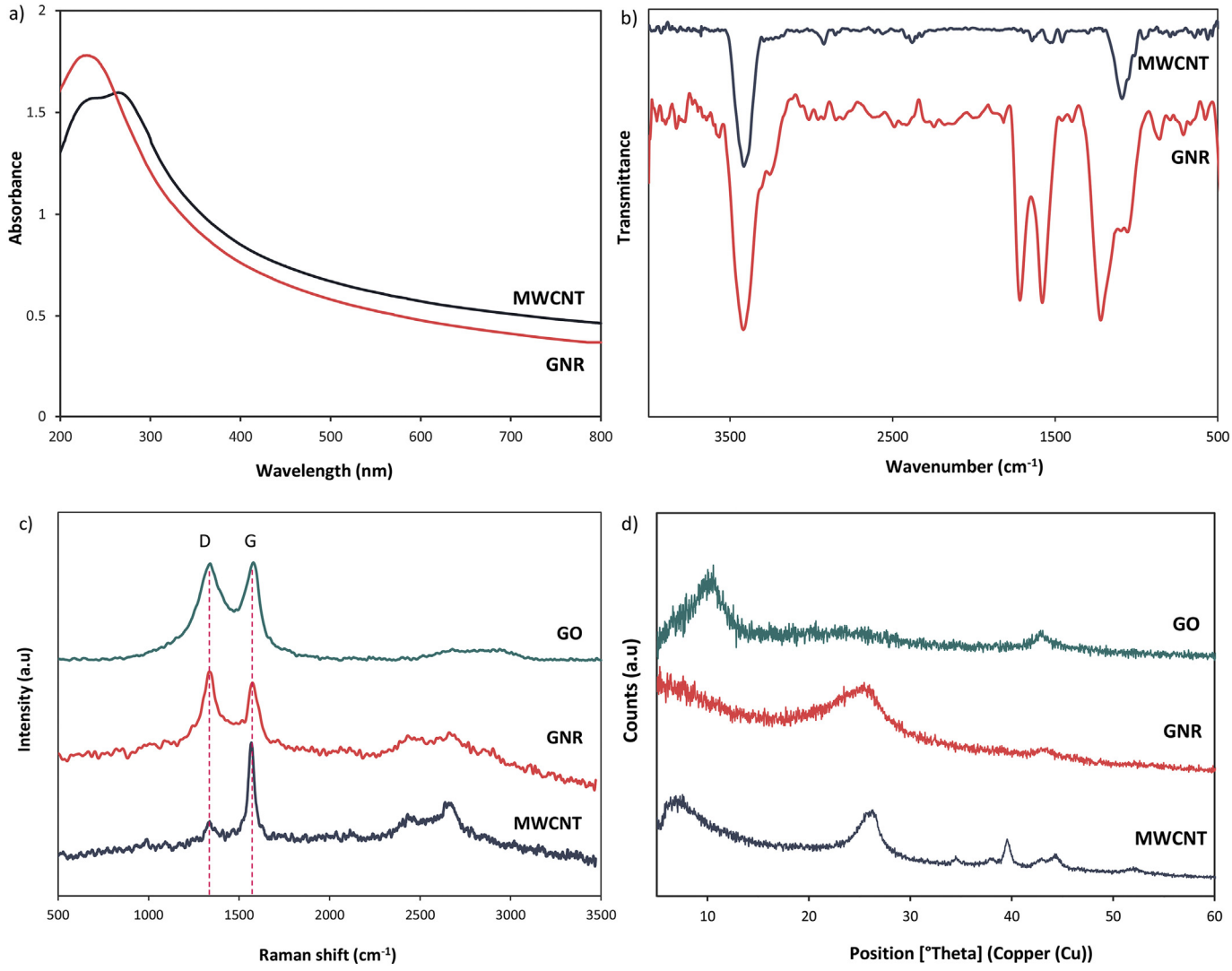

Fig. 1. a) UV–Vis spectra; b) FTIR spectra of MWCNT and GNR; c) Raman spectra; d) XRD pattern of MWCNT,GNR and GO structures.

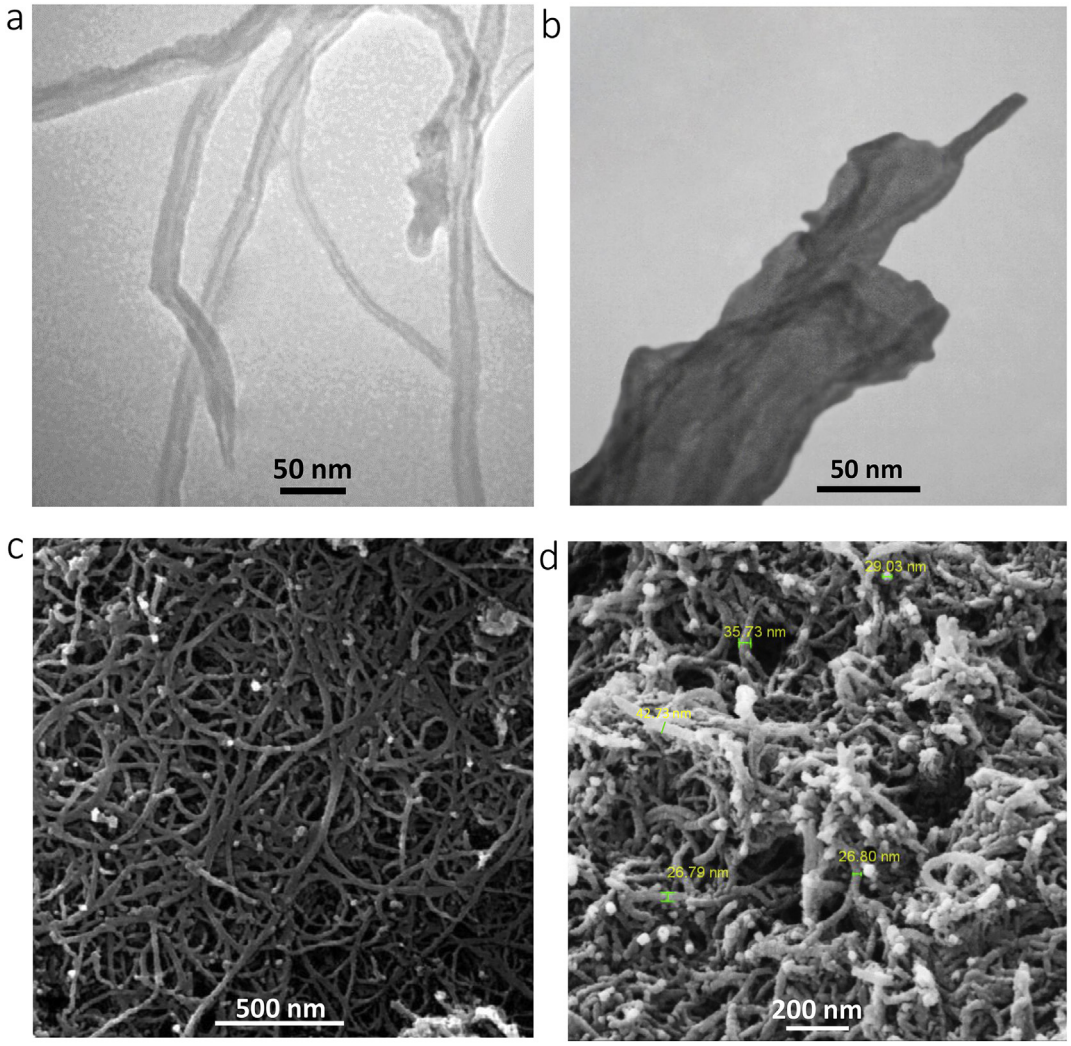

Fig. 2. The TEM image of a) MWCNT, b) the synthesized GNR; FESEM image of c) MWCNT and d) GNR.

3.2. Catalytic activity of GNR compare to GO and MWCNT

To evaluate the peroxidase-like activity of GNR and comparing its catalytic ability with GO and MWCNT, a given concentration of each nanostructure was added to NaOAC-HOAC buffer. The absorption spectrum of each mixture was recorded 10 min after addition of H_2O_2 and TMB. According to Fig. 3a and b, the absorption intensity was increased for all three nanostructures indicating the ability of GNR, GO and MWCNT to catalyze the oxidation of TMB in the presence of H_2O_2. This catalyzed oxidation process leads to the formation of a blue color product, oxidized TMB (oxTMB). However, as expected, the experiments proved that GNR exhibits superior catalytic activity towards the oxidation of TMB (Fig. 3a). Indeed, it can be concluded that smaller size of nanoribbons compare to graphene sheets, higher density of oxygen-containing functionalities, rich edge and defect density could be responsible for the acceleration of electron transfer in GNR which can result in its higher catalytic activity [31,32,60,61]. Interestingly, rapid electron transfer in GNR leads to the enhanced and speeded up redox reaction between TMB and H_2O_2 [62]. Moreover, it can reasonably be assumed that GNR can display excellent electrocatalytic activity over MWCNT due to its larger active surface area, more open-ended structures, higher edge-plane and electrochemically active sites [60]. Consequently, these findings point to the high catalytic action of GNR over GO and MWCNT.

According to the studies and peroxidase-like activity of most enzyme mimics [3,4], the catalytic ability of GNR may be driven by increasing the electron density of GNR. It can occur due to electron transfer from ion-pair electrons in amino groups of TMB to GNR. This leads to the acceleration of the electron transfer from GNR to H_2O_2 and would result in an increase in the production of OH radicals. Therefore, TMB oxidation rate in the presence of the produced OH radicals would speed up [19,22]. In the first step, H_2O_2 molecules are adsorbed on the surface of GNR. At this point, GNR, as a peroxidase, catalyzes the H_2O_2 decomposition and produces OH radicals. Furthermore, the generated OH radicals could be stabilized on the surface of GNR due to electron exchange interaction. In the next step, OH radicals participate in the redox reaction and produce oxTMB which is responsible for the blue color of the solution [5,19,22]. In fact, the blue color of the oxTMB is observed because of the formation of a charge transfer complex between TMB and cation free radical TMB^+ [19].

The spectra and color change of the solutions as a result of oxTMB production in the presence of nanostructures and H_2O_2 are shown in Fig. 3b and c, respectively. As illustrated in Fig. 3b, there is a weak broad absorption band at 650–700 nm originated from TMB oxidation in the presence of H_2O_2 in the mixture of buffer, H_2O_2 and TMB as blank and its attributed solution appeared colorless (Fig. 3c, solution 1). However, the observed absorption bands at 653 nm originate from TMB-H_2O_2 reaction in the presence of MWCNT, GO and GNR which indicate the catalytic behavior of these carbon-based nanostructures. In addition, it is clear that considerable TMB oxidation occurred in the

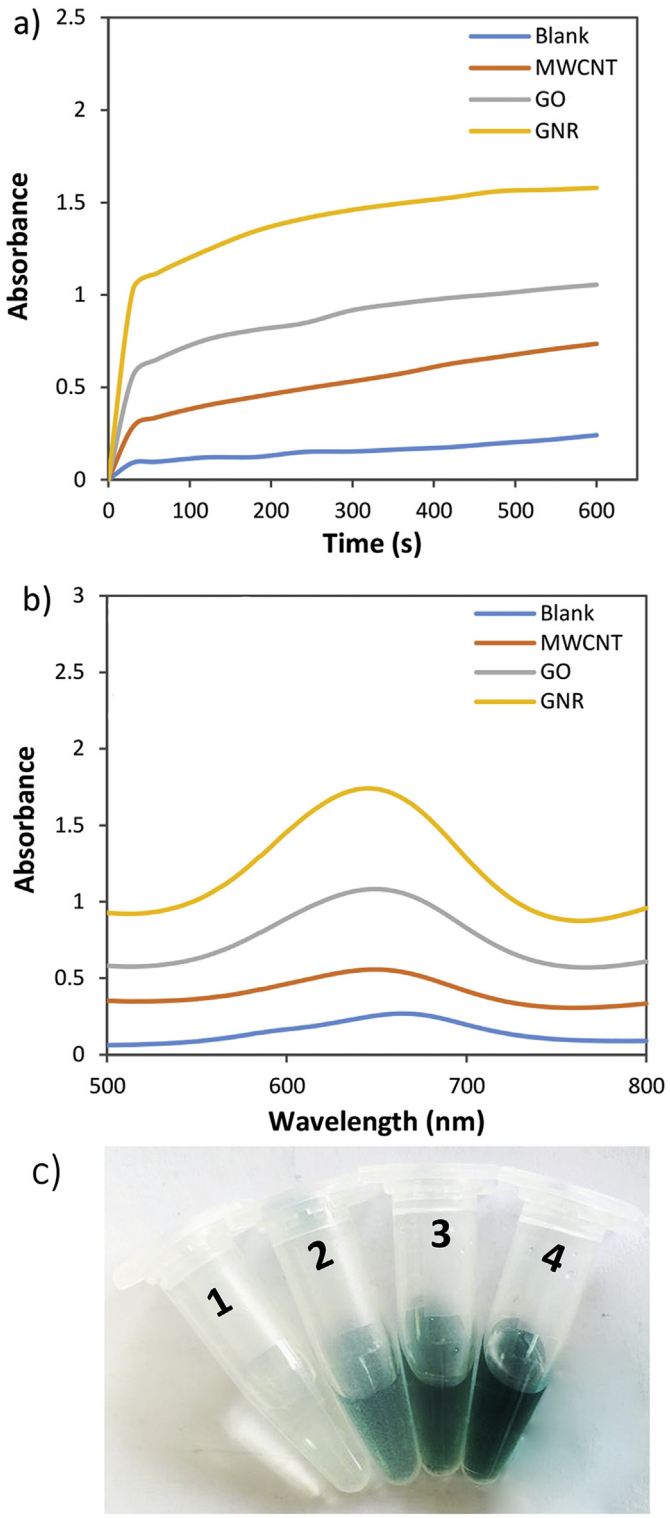

Fig. 3. Comparison of peroxidase-like activity of GNR, GO and MWCNT; a) The time-dependent UV–Vis absorption changes at 653 nm in the presence of nanostructures (0.5 mg mL^{-1}), H_2O_2 (50 mM) and TMB (5 mM), b) The UV–Vis absorption spectra of blank and other different systems in the presence of GNR, GO and MWCNT, c) The photograph of the corresponding solutions 1. blank (buffer, H_2O_2 and TMB), 2. MWCNT, 3. GO and 4. GNR.

presence of GNR. The color change from colorless to blue in solutions 2, 3 and 4 (Fig. 3c) again proves the production of oxTMB in the presence of MWCNT, GO and GNR, respectively. Moreover, based on the spectra and color of the solutions, it can clearly be concluded that GNR as an artificial nanozyme displays exceptional peroxidase-like activity and leads to produce more oxTMB and deep blue color (solution 4), while no color change was observed in the blank (solution 1). Also, in comparison to GNR, the solutions with lighter blue colors were obtained in the presence of MWCNT (solution 2) and GO (solution 3).

3.3. Optimization of peroxidase-like activity of GNR

The peroxidase-like activity of most nanozymes depends on the pH, temperature, incubation time and amount of nanostructures. Hence, the enzyme-like activity of GNR was investigated under different conditions and the absorbance changes at 653 nm were recorded upon different pH (2 − 10), temperature (20–50 °C), GNR concentration (0.01–0.5 mg mL^{-1}) and time (5–30 min).

In order to verify the impact of pH, the absorption changes of oxTMB at 653 nm were recorded in the pH range of 2–10. As shown in Fig. 4a, the highest ΔA (ΔA = A-A_0) and catalytic activity were obtained at pH 4 while it was steady from pH 5 to 10. Also as can be seen in the inset image, the blue color of the oxTMB was observed at pH 4. Indeed, the catalytic reaction between TMB and H_2O_2 is slow at neutral and basic pH and no color change was observed in this pH range. In other words, H_2O_2 tends to decompose into H_2O and O_2 at pH > 4. As a result, lack of H_2O_2 which is the main source of active OH radicals leads to limited interaction between GNR and H_2O_2 and blocking the H_2O_2-TMB redox reaction [63]. So that, no oxTMB can be observed in the system at pH 5–10. Therefore, pH 4 was used as an optimized pH for further catalytic studies.

The reaction temperature is another important parameter that influences the catalytic activity of nanozymes. To study the impact of temperature, the mixture of buffer (NaOAC-HOAC 0.2 M, pH 4) and GNR were incubated for 10 min at different temperatures (20, 25, 30, 35, 40, 45 and 50 °C) after addition of H_2O_2 and TMB. According to the illustrated curve in Fig. 4b, the highest ΔA was obtained at 40 °C whereas it drastically decreased at higher temperatures. Thereupon, the catalytic reaction of TMB- H_2O_2 was carried out at 40 °C as the optimized temperature.

Different concentrations of GNR as nanozyme (0.01, 0.025, 0.05, 0.1, 0.25 and 0.5 mg mL^{-1}) were added to the mixture of the reaction and the absorption changes were recorded at 653 nm. As Fig. 4c displays, ΔA was increased up to 0.1 mg mL^{-1} of GNR and it was steady with a slight decrease at higher concentrations. Therefore, 0.1 mg mL^{-1} of GNR was used as the optimum concentration.

To identify the incubation time effect on the activity of the proposed nanozyme, the mixture of buffer and GNR was incubated for 5, 10, 15, 20, 25 and 30 min at 40 °C after the addition of H_2O_2 and TMB. As shown in Fig. 4d, the highest ΔA was obtained at 10 min incubation and a decrease in ΔA was observed until 30 min. Thus, the mixture was incubated for 10 min to investigate the catalytic activity of GNR.

3.4. Kinetic study of peroxidase-like activity of GNR

To understand the catalytic behavior of GNR more precisely, steady-state kinetic assays were performed in the presence of varied concentrations of H_2O_2 and TMB. The experiments were carried out according to the enzyme kinetics theory and methods in which one substrate remained at constant concentration while the concentration of other substrate was varied. As illustrated in Fig. 5, the typical Michaelis-Menten (Fig. 5a and b) and Lineweaver-Burk curves (Fig. 5c and d) were plotted at a given concentration range of H_2O_2 and TMB, respectively. According to the obtained results, it was revealed that the oxidation reaction catalyzed by GNR towards H_2O_2 and TMB follows the typical Michaelis-Menten model. The key enzymatic kinetic parameters including Michaelis-Menten constant (K_m) and the maximum reaction velocity (V_{max}) were determined by fitting the Lineweaver-Burk equation in double reciprocal plots. As known, K_m is a kinetic parameter to identify the enzyme affinity towards the substrates and a

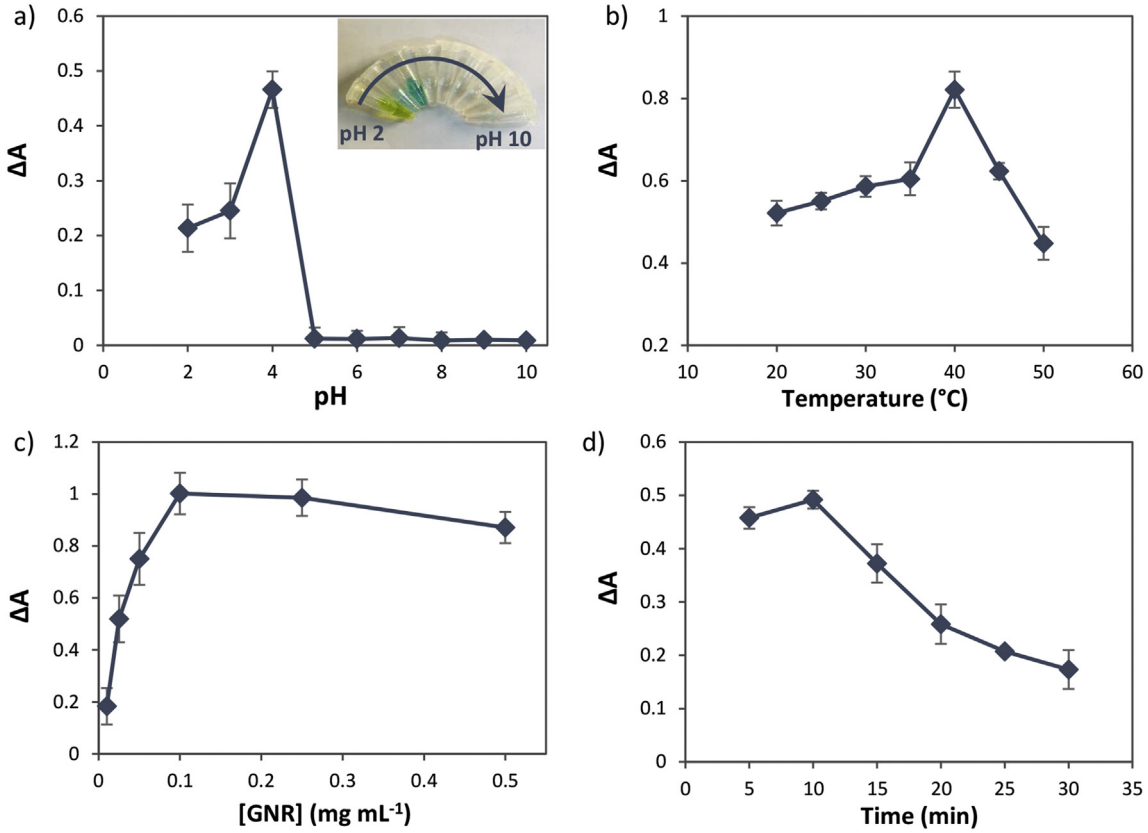

Fig. 4. Optimization of peroxidase-like activity of GNR; The impact of a) pH (2–10), b) temperature (20–50 °C), c) GNR concentration (0.01–0.5 mg mL^{-1}) and d) time (5–30 min) on ΔA (The concentration of NaOAC-HOAC, H_2O_2 and TMB were 0.2 M, 50 mM and 5 mM, respectively).

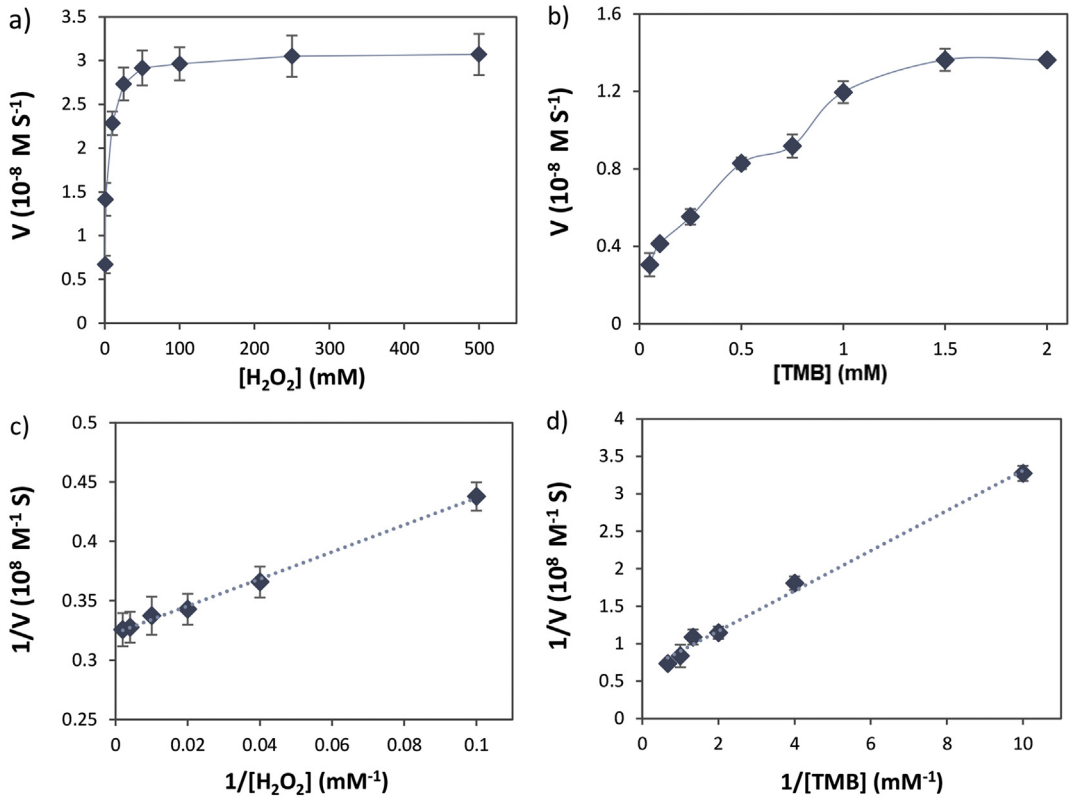

Fig. 5. The steady-state kinetic study of GNR; a) TMB concentration was constant at 2.5 mM and H_2O_2 concentration varied between 0.5 and 500 mM, b) H_2O_2 concentration was constant at 50 mM and TMB concentration varied between 0.05 and 2 mM. c, d) The corresponding Lineweaver-Burk plots of the double reciprocal of the Michaelis – Menten equation with the fixed concentration of one substrate and varied the other substrate.

Table 1
The apparent kinetic parameters of GNR in comparison with other catalysts.

Catalyst	K_m (mM)		V_m (10^{-8} MS^{-1})		Ref
	H_2O_2	TMB	H_2O_2	TMB	
HRP	3.7	0.43	8.71	10	[64]
Fe_3O_4	154	0.098	9.78	3.44	[64]
GO-COOH	3.99	0.0237	3.85	3.45	[65]
GO-Fe_3O_4	0.71	0.43	5.31	13.08	[26]
GNR	3.52	0.42	3.09	1.58	This study

low value of K_m represents higher enzyme affinity to a substrate and vice versa [26]. The K_m values of GNR for H_2O_2 and TMB were calculated 3.52 and 0.42 mM, respectively. As listed in Table 1, it was found that the obtained kinetic parameters for GNR are slightly smaller than the reported K_m for HRP enzyme (H_2O_2: 3.7 mM and TMB: 0.43 mM) [64] which prove high catalytic activity of GNR and consequently offer GNR as an adequate artificial enzyme for wide range of applications. Also, the K_m value of H_2O_2 for GNR was close to GO-COOH [65] and 44 times lower than that of Fe_3O_4 [64]. These results indicate that GNR exhibits higher affinity towards H_2O_2 over HRP, GO-COOH and Fe_3O_4, suggesting lower concentration of H_2O_2 is required for reaching to maximum peroxidase-like activity of GNR in comparison to other mentioned catalysts. Therefore, GNR can be applied as an excellent alternative to natural peroxidases.

3.5. Detection of DA using GNR as nanozyme

The enzyme mimic activity of label-free GNR as a nanozyme was applied for colorimetric detection of DA under the optimum condition. To this aim, different concentrations of DA were added to the mixture of buffer and GNR solution and the changes of oxTMB absorption were recorded at 653 nm. DA with the reducing function could consume H_2O_2 through a redox reaction. It leads to inhibition of TMB oxidation in the presence of H_2O_2 on the surface of GNR. Therefore, increasing the concentration of DA with an inhibitory effect on the oxidation of TMB resulted in less producing of oxTMB, which is associated with decrease in A_{653} and diminish in blue color of the solution. Under this condition, the solution remains colorless at a high concentration of DA due to inhibition of TMB oxidation. Fig. 6 schematically outlines this possible strategy of DA detection.

To clarify this strategy, the changes in the UV–Vis spectra (Fig. 7a) of oxTMB were recorded in the presence of different concentrations of DA, ranged from 0 to 1000 μM. Moreover, the correspond color changes of the solution, due to the changing of DA concentrations, can be observed in Fig. 7a (inset) which clearly shows the fading of deep blue color of the solution by increasing the concentration of DA. This color changing proves the ability of the proposed nanozyme in colorimetric detection of DA visually and by naked eyes. Utilizing the obtained A_{653} through changing DA concentration, a typical calibration curve was plotted in the concentration range from 0 to 1000 μM. Also, two good linear relationships were observed between a decrease in A_{653} and increment in DA concentration ranges of 0.1–1 μM with linear equation of $A_{653} = -0.0989C + 0.5608$ ($R^2 = 0.9968$) and 2.5–50 μM with linear equation of $A_{653} = -0.0067 + 0.4711$ ($R^2 = 0.9975$) (Fig. 7b). Considering the linear equation in the concentration level of 0.1–1 μM (Fig. 7b, inset), the limit of detection (LOD) was calculated 0.035 μM using the slope of the calibration curve (m) and standard deviation of y-intercept (σ). The obtained analytical parameters of this study were summarized in Table 2 and compared to the linear range and LOD of some previously reported methods. According to Table 2, the proposed peroxidase-like mimic exhibited excellent sensitivity and low LOD compared to some electrochemical [42,48,49] and fluorescence sensors [52] and other reported artificial nanozymes in the literature [66–76]. Although there are some highly sensitive electrochemical and fluorescence sensors with LODs in nM level [44,51] which show that the proposed method still needs more modification to provide higher sensitivity, but in most cases the LODs are higher than the LOD of this work. As an explanation, the improved sensitivity can be due to the high density of edge defects and accelerated electron transfer in GNR. In other words, fast electron transfer is responsible for increasing the rate of redox reaction [62,77]. Therefore, GNR displays higher catalytic performance and enhanced sensitivity in comparison to other reported nanozymes in the paper. As a matter of fact, this finding provides additional support for the successful application of GNR as a nanozyme which its combination with other catalytically active nanostructures would offer a synergic effect and extreme enhancement in catalytic activity and sensing approaches. In fact, hybridization of GNR with other catalytically active nanomaterials would be beneficial for developing a new enhanced sensing platform for further studies especially when detection of molecules in trace concentrations is essential. The reproducibility of the present sensing method for DA detection was examined by five parallel measurements of 25 μM DA and the RSD% was estimated about 3.7%. Also, the catalytic activity of three different batches of GNR was determined and RSD% was found to be 5.0%. To study the long-term stability, the peroxidase-like activity of GNR towards TMB oxidation was investigated during 5 month-storage of GNR and RSD% was obtained as 1% which demonstrates good long-term stability of GNR.

3.6. The selectivity of colorimetric method

In order to further evaluation of the proposed sensor selectivity towards DA, several potential interfering compounds and biomaterials including glutamic acid (Glu), cysteine (Cys), tryptophan (Trp), phenylalanine (Phe), ascorbic acid (AA), glucose (Gluc), uric acid (UA),

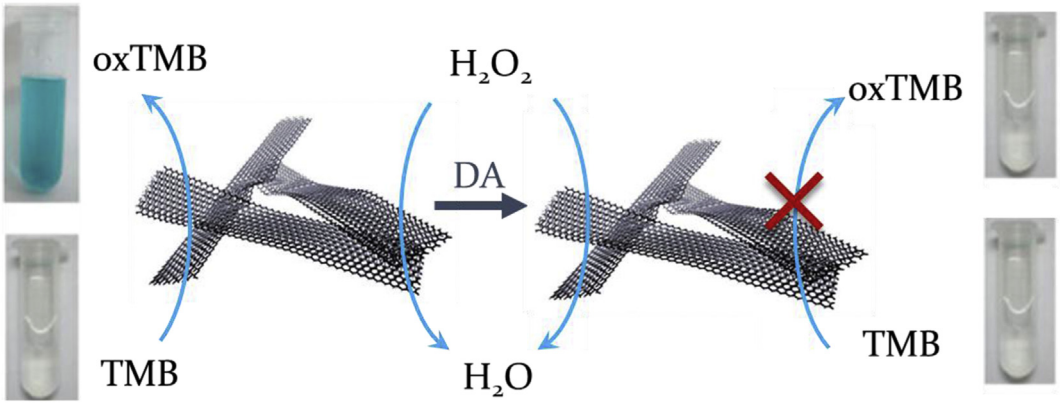

Fig. 6. Schematic mechanism of DA detection.

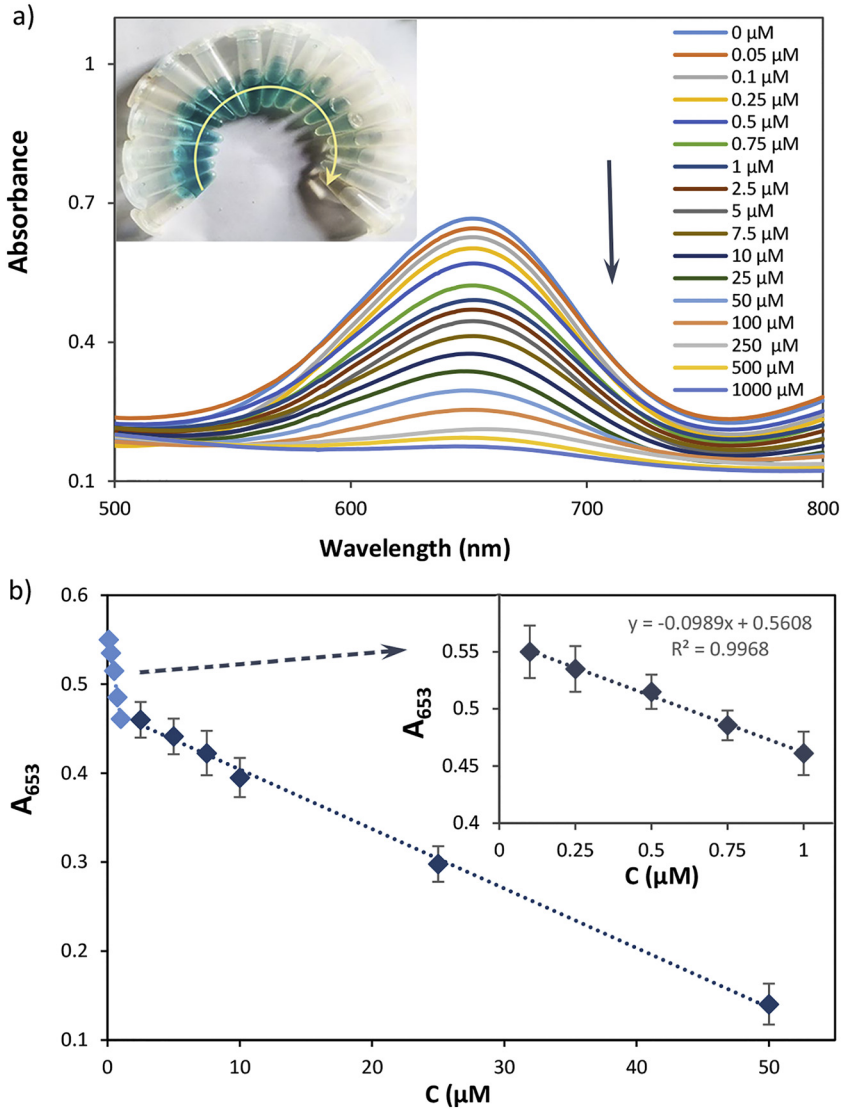

Fig. 7. a) The UV–Vis spectra of the produced oxTMB in the presence of GNR and varied concentrations of DA (0. 0.05, 0.1, 0.25, 0.5, 0.75, 1, 2.5, 5, 7.5, 10, 25, 50, 100, 250, 500 and 1000 µM); Inset: The photograph of the corresponding color changes, b) The calibration curve of A_{653} changes vs. different concentrations of DA in the range of 0.1–50 µM; Inset: The linear calibration curve of DA in the range of 0.1–1 µM, (In all experiments NaOAC-HOAC 0.2 M pH 4, H_2O_2 (50 mM) and TMB (2.5 mM)) were used.

Table 2
Comparison of GNR with the previously introduced sensors for detection of DA.

Nanomaterials	Detection strategy	Linear range (µM)	Detection limit (µM)	Ref
Nanoporous Au microelectrode	Electrochemical	0.1–10	0.03	[42]
Cu_2O-RGO/GCE	Electrochemical	0.01–1, 1–80	0.006	[44]
CuO/g-C_3N_4	Electrochemical	0.2–16, 16–78.7	0.06	[48]
Au-ZnO NCAs/GF	Electrochemical	0–80	0.04	[49]
MoS_2 QDNS	Fluorescence	0.0025–5, 5–10.4	0.0009	[51]
N-CQDs	Fluorescence	0.05–15	0.035	[52]
β-CD-Au NPs	Colorimetric/assembly	0.02–0.25 and 0.35–1.6	0.003	[66]
Au NRs	Colorimetric/aggregation	0.1–1, 1–10 and 10–10,000	0.03	[67]
TSIL-Ag NPs	Colorimetric/etching	0.1–7.5	0.031	[68]
CuS/rGO	Colorimetric/nanozyme	2–200	0.48	[69]
Co-MGNCs	Colorimetric/nanozyme	0.5–50	0.08	[70]
Pt/hBNNSs	Colorimetric/nanozyme	2–55	0.76	[71]
$CoFe_2O_4$/CoS	Colorimetric/nanozyme	0–50	0.58	[72]
Co_3O_4/CuO HNCs	Colorimetric/nanozyme	0.05–8	0.027	[73]
Cu-MOXs	Colorimetric/nanozyme	0.5–20	0.86	[74]
$CuFe_2O_4/Cu_9S_8$/PPy	Colorimetric/nanozyme	2–20	1.0	[75]
h-CuS NCs	Colorimetric/nanozyme	2–150	1.67	[76]
GNR	Colorimetric/nanozyme	0.1–1, 2.5–50	0.035	This study

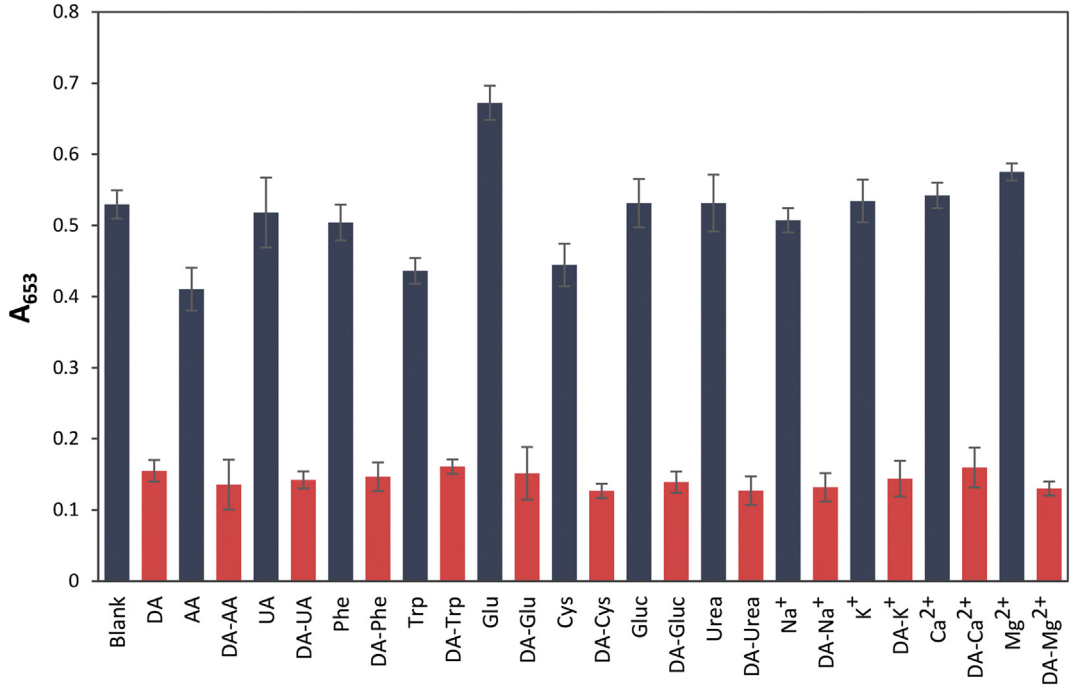

Fig. 8. The selectivity of the GNR towards DA and some potential interfering substances (dark blue bars) and their binary mixture with DA (red bars). (For interpretation of the references to color in this figure legend, the reader is referred to the web version of this article.)

urea and cations (Na^+, K^+, Cu^{2+}, Ca^{2+}, Mg^{2+}) were introduced to the above described sensing system and their corresponding responses were investigated both individually and in combination with DA. As expected, the quenching of the oxidation process was observed only in the presence of DA (Fig. 8) and other studied compounds exhibited no significant interfering effect even up to 10 mM (by a factor of 100-fold). The recoveries of DA in the binary mixtures of DA and each potential interfering compound were in the range of 92.6–102.7% and the relative errors (%) were found to be in range of 0.14–8.0%. It seems that more effective interactions between DA and GNR rather than those between the potential interfering compounds and GNR, strong DA chemisorption on the GNR surface and its edges, and high reduction potential of DA are the main reasons for good selectivity of the present sensing method for DA detection over other potential interfering species. This result suggests that GNR as a label-free nanozyme and colorimetric sensing probe can be employed for selective detection of DA.

3.7. Detection of DA in real sample

The ability of GNR for DA assay in human serum sample was investigated. To this attention, various amounts of DA standard solution were spiked to the diluted serum samples and the solutions of DA in serum samples were prepared with the final concentration of 0.2, 0.4 and 0.8 μM. The prepared spiked serum samples were introduced to the described sensor and were determined based on the catalytic activity of GNR. Considering summarized data in Table 3, the relative recoveries for DA quantification were achieved in the range of 90–110% with RSD % < 7.8%. These results offer further evidence for successful detection of DA in biological samples using GNR as a colorimetric sensor and demonstrate that the proposed nanozyme can be satisfactorily applied in complex matrices with no significant interfering effect.

Table 3
Determination of DA in human serum samples using GNR as nanozyme.

Sample	Spiked amount (μM)	Founded (μM)	Recovery (%)	RSD (%, n = 3)
Serum 1	0.2	0.19	95	7
	0.4	0.37	92.5	7.8
	0.8	0.87	108.7	5.2
Serum 2	0.2	0.19	95	5.6
	0.4	0.42	105	3.2
	0.8	0.88	110	4.5
Serum 3	0.2	0.18	90	3.5
	0.4	0.41	102.5	4.5
	0.8	0.86	107.5	3.1

4. Conclusion

The peroxidase-like activity of GNR and its application as a colorimetric platform for DA sensing was successfully investigated. The findings of this study demonstrated that GNR exhibited higher catalytic activity over GO and MWCNT, due to its exceptional structural properties. Based upon the excellent catalytic performance of GNR, a label-free colorimetric sensor was developed for simple and selective detection of DA with a low detection limit and wide linear range. Detection of DA by utilizing the catalyzed TMB-H_2O_2 redox reaction on GNR was performed according to the inhibitory effect of DA on TMB oxidation reaction. This approach provides great potential application and a beneficial impact on various fields such as biosensing, bioanalysis and clinical diagnosis.

Supplementary data to this article can be found online at https://doi.org/10.1016/j.msec.2020.111034.

CRediT authorship contribution statement

Simindokht Rostami: Conceptualization, Investigation, Methodology, Validation, Visualization, Writing - original draft. **Ali Mehdinia:** Supervision, Resources, Writing - review & editing. **Ali Jabbari:** Project administration, Resources, Funding acquisition, Writing - review & editing.

Declaration of competing interest

The authors declare that they have no known competing financial

interests or personal relationships that could have appeared to influence the work reported in this paper.

Acknowledgment

We are thankful to the Department of Analytical Chemistry, Faculty of Chemistry, K.N.Toosi University of Technology, Tehran, Iran. We also gratefully acknowledge the financial support for this work by the Iran National Science Foundation (INSF) with grant number of 96012764.

References

[1] L. Tang, J. Li, Plasmon-based colorimetric nanosensors for ultrasensitive molecular diagnostics, ACS Sensors 2 (7) (2017) 857–875.
[2] J. Wang, X. Qu, Recent progress in nanosensors for sensitive detection of biomolecules, Nanoscale 5 (9) (2013) 3589–3600.
[3] H. Wei, E. Wang, Nanomaterials with enzyme-like characteristics (nanozymes): next-generation artificial enzymes, Chem. Soc. Rev. 42 (14) (2013) 6060–6093.
[4] J. Wu, X. Wang, Q. Wang, Z. Lou, S. Li, Y. Zhu, L. Qin, H. Wei, Nanomaterials with enzyme-like characteristics (nanozymes): next-generation artificial enzymes (II), Chem. Soc. Rev. 48 (4) (2019) 1004–1076.
[5] H. Wang, K. Wan, X. Shi, Recent advances in nanozyme research, Adv. Mater. 31 (45) (2018) 1805368–1805377.
[6] M. Liang, X. Yan, Nanozymes: from new concepts, mechanisms, and standards to applications, Acc. Chem. Res. 52 (8) (2019) 2190–2200.
[7] Y. Zhou, B. Liu, R. Yang, J. Liu, Filling in the gaps between nanozymes and enzymes: challenges and opportunities, Bioconjug. Chem. 28 (12) (2017) 2903–2909.
[8] Y. Huang, J. Ren, X. Qu, Nanozymes: classification, catalytic mechanisms, activity regulation, and applications, Chem. Rev. 119 (6) (2019) 4357–4412.
[9] X. Wang, Y. Hu, H. Wei, Nanozymes in bionanotechnology: from sensing to therapeutics and beyond, Inorg Chem Front 3 (1) (2016) 41–60.
[10] B. Garg, T. Bisht, Y.-C. Ling, Graphene-based nanomaterials as efficient peroxidase mimetic catalysts for biosensing applications: an overview, Molecules 20 (8) (2015) 14155–14190.
[11] S. Liu, J. Tian, L. Wang, Y. Luo, G. Chang, X. Sun, Iron-substituted SBA-15 microparticles: a peroxidase-like catalyst for H_2O_2 detection, Analyst 136 (23) (2011) 4894–4897.
[12] S. Liu, J. Tian, L. Wang, Y. Zhang, Y. Luo, H. Li, A.M. Asiri, A.O. Al-Youbi, X. Sun, Fast and sensitive colorimetric detection of H_2O_2 and glucose: a strategy based on polyoxometalate clusters, ChemPlusChem 77 (7) (2012) 541–544.
[13] S. Liu, J. Tian, L. Wang, X. Sun, Highly sensitive and selective colorimetric detection of Ag (I) ion using 3, 3′, 5, 5′,-tetramethylbenzidine (TMB) as an indicator, Sensor Actuat B: Chem 165 (1) (2012) 44–47.
[14] Q. Zhong, Y. Chen, A. Su, Y. Wang, Synthesis of catalytically active carbon quantum dots and its application for colorimetric detection of glutathione, Sensor Actuat B: Chem 273 (2018) 1098–1102.
[15] V.K. Singh, P.K. Yadav, S. Chandra, D. Bano, M. Talat, S.H. Hasan, Peroxidase mimetic activity of fluorescent NS-carbon quantum dots and their application in colorimetric detection of H_2O_2 and glutathione in human blood serum, J. Mater. Chem. B 6 (32) (2018) 5256–5268.
[16] M. Shamsipur, A. Safavi, Z. Mohammadpour, Indirect colorimetric detection of glutathione based on its radical restoration ability using carbon nanodots as nanozymes, Sensor Actuat B: Chem 199 (2014) 463–469.
[17] L. Zhao, Z. Wu, G. Liu, H. Lu, Y. Gao, F. Liu, C. Wang, J. Cui, G. Lu, High-activity Mo, S co-doped carbon quantum dot nanozyme-based cascade colorimetric biosensor for sensitive detection of cholesterol, J. Mater. Chem. B 7 (44) (2019) 7042–7051.
[18] S. Liu, J. Tian, L. Wang, Y. Luo, X. Sun, A general strategy for the production of photoluminescent carbon nitride dots from organic amines and their application as novel peroxidase-like catalysts for colorimetric detection of H_2O_2 and glucose, RSC Adv. 2 (2) (2012) 411–413.
[19] J. Qian, X. Yang, Z. Yang, G. Zhu, H. Mao, K. Wang, Multiwalled carbon nanotube@ reduced graphene oxide nanoribbon heterostructure: synthesis, intrinsic peroxidase-like catalytic activity, and its application in colorimetric biosensing, J. Mater. Chem. B 3 (8) (2015) 1624–1632.
[20] Y. Song, X. Wang, C. Zhao, K. Qu, J. Ren, X. Qu, Label-free colorimetric detection of single nucleotide polymorphism by using single-walled carbon nanotube intrinsic peroxidase-like activity, Chem. Eur. J. 16 (12) (2010) 3617–3621.
[21] Y. He, X. Niu, L. Shi, H. Zhao, X. Li, W. Zhang, J. Pan, X. Zhang, Y. Yan, M. Lan, Photometric determination of free cholesterol via cholesterol oxidase and carbon nanotube supported Prussian blue as a peroxidase mimic, Microchim. Acta 184 (7) (2017) 2181–2189.
[22] N.R. Nirala, S. Abraham, V. Kumar, A. Bansal, A. Srivastava, P.S. Saxena, Colorimetric detection of cholesterol based on highly efficient peroxidase mimetic activity of graphene quantum dots, Sensor Actuat B: Chem 218 (2015) 42–50.
[23] L. Zhang, X. Hai, C. Xia, X.-W. Chen, J.-H. Wang, Growth of CuO nanoneedles on graphene quantum dots as peroxidase mimics for sensitive colorimetric detection of hydrogen peroxide and glucose, Sensor Actuat B: Chem 248 (2017) 374–384.
[24] H.V. Tran, T.A. Le, B.L. Giang, B. Piro, L. Dai Tran, Silver nanoparticles on graphene quantum dots as nanozyme for efficient H_2O_2 reduction in a glucose biosensor, Mater. Res. Express 6 (11) (2019) 115403–115410.
[25] X.-Q. Lin, H.-H. Deng, G.-W. Wu, H.-P. Peng, A.-L. Liu, X.-H. Lin, X.-H. Xia, W. Chen, Platinum nanoparticles/graphene-oxide hybrid with excellent peroxidase-like activity and its application for cysteine detection, Analyst 140 (15) (2015) 5251–5256.
[26] Y.-l. Dong, H.-g. Zhang, Z.U. Rahman, L. Su, X.-j. Chen, J. Hu, X.-g. Chen, Graphene oxide–Fe_3O_4 magnetic nanocomposites with peroxidase-like activity for colorimetric detection of glucose, Nanoscale 4 (13) (2012) 3969–3976.
[27] G. Darabdhara, B. Sharma, M.R. Das, R. Boukherroub, S. Szunerits, Cu-Ag bimetallic nanoparticles on reduced graphene oxide nanosheets as peroxidase mimic for glucose and ascorbic acid detection, Sensor Actuat B: Chem 238 (2017) 842–851.
[28] P.-C. Lee, N.-S. Li, Y.-P. Hsu, C. Peng, H.-W. Yang, Direct glucose detection in whole blood by colorimetric assay based on glucose oxidase-conjugated graphene oxide/MnO_2 nanozymes, Analyst 144 (9) (2019) 3038–3044.
[29] Y. Guo, L. Deng, J. Li, S. Guo, E. Wang, S. Dong, Hemin− graphene hybrid nanosheets with intrinsic peroxidase-like activity for label-free colorimetric detection of single-nucleotide polymorphism, ACS Nano 5 (2) (2011) 1282–1290.
[30] J. Zhu, W. Nie, Q. Wang, J. Li, H. Li, W. Wen, T. Bao, H. Xiong, X. Zhang, S. Wang, In situ growth of copper oxide-graphite carbon nitride nanocomposites with peroxidase-mimicking activity for electrocatalytic and colorimetric detection of hydrogen peroxide, Carbon 129 (2018) 29–37.
[31] V. Mani, M. Govindasamy, S.-M. Chen, T.-W. Chen, A.S. Kumar, S.-T. Huang, Core-shell heterostructured multiwalled carbon nanotubes@ reduced graphene oxide nanoribbons/chitosan, a robust nanobiocomposite for enzymatic biosensing of hydrogen peroxide and nitrite, Sci. Rep. 7 (1) (2017) 11910–11919.
[32] U. Rajaji, R. Arumugam, S.-M. Chen, T.-W. Chen, T.-W. Tseng, S. Chinnapaiyan, S.-Y. Lee, W.-H. Chang, Graphene nanoribbons in electrochemical sensors and biosensors: a review, Int. J. Electrochem. Sci. 13 (2018) 6643–6654.
[33] A.L. Higginbotham, D.V. Kosynkin, A. Sinitskii, Z. Sun, J.M. Tour, Lower-defect graphene oxide nanoribbons from multiwalled carbon nanotubes, ACS Nano 4 (4) (2010) 2059–2069.
[34] S. Sandeep, A.S. Santhosh, N.K. Swamy, G.S. Suresh, J.S. Melo, N.A. Chamaraja, A biosensor based on a graphene nanoribbon/silver nanoparticle/polyphenol oxidase composite matrix on a graphite electrode: application in the analysis of catechol in green tea samples, New J. Chem. 42 (20) (2018) 16620–16629.
[35] W. Yuan, Y. Zhou, Y. Li, C. Li, H. Peng, J. Zhang, Z. Liu, L. Dai, G. Shi, The edge-and basal-plane-specific electrochemistry of a single-layer graphene sheet, Sci. Rep. 3 (2013) 2248–2254.
[36] Q. He, Y. Tian, Y. Wu, J. Liu, G. Li, P. Deng, D. Chen, Facile and ultrasensitive determination of 4-nitrophenol based on acetylene black paste and graphene hybrid electrode, Nanomaterials 9 (3) (2019) 429–444.
[37] Q. He, Y. Wu, Y. Tian, G. Li, J. Liu, P. Deng, D. Chen, Facile electrochemical sensor for nanomolar rutin detection based on magnetite nanoparticles and reduced graphene oxide decorated electrode, Nanomaterials 9 (1) (2019) 115–130.
[38] R.M. Wightman, L.J. May, A.C. Michael, Detection of dopamine dynamics in the brain, Anal. Chem. 60 (13) (1988) 769A–793A.
[39] M. El-Ghundi, B.F. O'Dowd, S.R. George, Insights into the role of dopamine receptor systems in learning and memory, Rev. Neurosci. 18 (1) (2007) 37–66.
[40] D.L. Robinson, A. Hermans, A.T. Seipel, R.M. Wightman, Monitoring rapid chemical communication in the brain, Chem. Rev. 108 (7) (2008) 2554–2584.
[41] T. Kienast, A. Heinz, Dopamine and the diseased brain, CNS Neurol Disord Drug Targets 5 (1) (2006) 109–131.
[42] H.S.C. Sáenz, L.P. Hernández-Saravia, J.S. Selva, A. Sukeri, P.J. Espinoza-Montero, M. Bertotti, Electrochemical dopamine sensor using a nanoporous gold microelectrode: a proof-of-concept study for the detection of dopamine release by scanning electrochemical microscopy, Microchim. Acta 185 (8) (2018) 367–375.
[43] Q. He, J. Liu, X. Liu, G. Li, D. Chen, P. Deng, J. Liang, A promising sensing platform toward dopamine using MnO_2 nanowires/electro-reduced graphene oxide composites, Electrochim. Acta 296 (2019) 683–692.
[44] Q. He, J. Liu, X. Liu, G. Li, P. Deng, J. Liang, Preparation of Cu_2O-reduced graphene nanocomposite modified electrodes towards ultrasensitive dopamine detection, Sensors 18 (1) (2018) 199–211.
[45] Q. He, J. Liu, X. Liu, G. Li, D. Chen, P. Deng, J. Liang, Fabrication of amine-modified magnetite-electrochemically reduced graphene oxide nanocomposite modified glassy carbon electrode for sensitive dopamine determination, Nanomaterials 8 (4) (2018) 194–208.
[46] Q. Li, Y. Xia, X. Wan, S. Yang, Z. Cai, Y. Ye, G. Li, Morphology-dependent MnO_2/nitrogen-doped graphene nanocomposites for simultaneous detection of trace dopamine and uric acid, Mater. Sci. Eng. C 109 (2020) 110615–110625.
[47] X. Guo, H. Yue, S. Song, S. Huang, X. Gao, H. Chen, P. Wu, T. Zhang, Z. Wang, Simultaneous electrochemical determination of dopamine and uric acid based on MoS2nanoflowers-graphene/ITO electrode, Microchem. J. 154 (2020) 104527.
[48] Y. Huang, Y. Tan, C. Feng, S. Wang, H. Wu, G. Zhang, Synthesis of CuO/gC_3N_4 composites, and their application to voltammetric sensing of glucose and dopamine, Microchim. Acta 186 (1) (2019) 10–18.
[49] H.Y. Yue, H.J. Zhang, S. Huang, X.X. Lu, X. Gao, S.S. Song, Z. Wang, W.Q. Wang, E.H. Guan, Highly sensitive and selective dopamine biosensor using Au nanoparticles-ZnO nanocone arrays/graphene foam electrode, Mater. Sci. Eng. C 108 (2020) 110490.
[50] H.Y. Yue, P.F. Wu, S. Huang, Z.Z. Wang, X. Gao, S.S. Song, W.Q. Wang, H.J. Zhang, X.R. Guo, Golf ball-like MoS_2 nanosheet arrays anchored onto carbon nanofibers for electrochemical detection of dopamine, Microchim. Acta 186 (6) (2019) 378–384.
[51] N.P. Mani, M. Ganiga, J. Cyriac, MoS_2 nanohybrid as a fluorescence sensor for highly selective detection of dopamine, Analyst 143 (7) (2018) 1691–1698.
[52] R. Zhang, Z. Fan, Nitrogen-doped carbon quantum dots as a "turn off-on" fluorescence sensor based on the redox reaction mechanism for the sensitive detection of dopamine and alpha lipoic acid, J. Photochem. Photobiol. A 392 (2020) 112438.

[53] V. Carrera, E. Sabater, E. Vilanova, M.A. Sogorb, A simple and rapid HPLC–MS method for the simultaneous determination of epinephrine, norepinephrine, dopamine and 5-hydroxytryptamine: application to the secretion of bovine chromaffin cell cultures, J. Chromatogr. B 847 (2) (2007) 88–94.
[54] P.A. Rasheed, J.-S. Lee, Recent advances in optical detection of dopamine using nanomaterials, Microchim. Acta 184 (5) (2017) 1239–1266.
[55] W. Li, J. Wang, J. Zhu, Y.-Q. Zheng, Co_3O_4 nanocrystals as an efficient catalase mimic for the colorimetric detection of glutathione, J. Mater. Chem. B 6 (42) (2018) 6858–6864.
[56] I. Bazin, S.A. Tria, A. Hayat, J.-L. Marty, New biorecognition molecules in biosensors for the detection of toxins, Biosens. Bioelectron. 87 (2017) 285–298.
[57] L. Shang, F. Zhao, B. Zeng, Highly dispersive hollow PdAg alloy nanoparticles modified ionic liquid functionalized graphene nanoribbons for electrochemical sensing of nifedipine, Electrochim. Acta 168 (2015) 330–336.
[58] D.C. Marcano, D.V. Kosynkin, J.M. Berlin, A. Sinitskii, Z. Sun, A. Slesarev, L.B. Alemany, W. Lu, J.M. Tour, Improved synthesis of graphene oxide, ACS Nano 4 (8) (2010) 4806–4814.
[59] S. Jovanović, T. Da Ross, A. Ostric, D. Tošić, J. Prekodravac, Z. Marković, B.T. Marković, Raman spectroscopy of graphene nanoribbons synthesized by longitudinal unzipping of multiwall carbon nanotubes, Phys. Scr. 2014 (T162) (2014) 014023–014026.
[60] M. Govindasamy, V. Mani, S.-M. Chen, T. Maiyalagan, S. Selvaraj, T.-W. Chen, S.-Y. Lee, W.-H. Chang, Highly sensitive determination of non-steroidal anti-inflammatory drug nimesulide using electrochemically reduced graphene oxide nanoribbons, RSC Adv. 7 (52) (2017) 33043–33051.
[61] G. Li, Y. Xia, Y. Tian, Y. Wu, J. Liu, Q. He, D. Chen, Review—recent developments on graphene-based electrochemical sensors toward nitrite, J. Electrochem. Soc. 166 (12) (2019) B881–B895.
[62] A. Liang, C. Li, D. Li, Y. Luo, G. Wen, Z. Jiang, A facile and sensitive peptide-modulating graphene oxide nanoribbon catalytic nanoplasmon analytical platform for human chorionic gonadotropin, Int. J. Nanomedicine 12 (2017) 8725–8734.
[63] J. Lian, P. Liu, X. Li, B. Bian, X. Zhang, Z. Liu, X. Zhang, G. Fan, L. Gao, Q. Liu, Multi-layer CeO_2-wrapped Ag_2S microspheres with enhanced peroxidase-like activity for sensitive detection of dopamine, Colloids Surf. A Physicochem. Eng. Asp. 565 (2019) 1–7.
[64] L. Gao, J. Zhuang, L. Nie, J. Zhang, Y. Zhang, N. Gu, T. Wang, J. Feng, D. Yang, S. Perrett, Intrinsic peroxidase-like activity of ferromagnetic nanoparticles, Nat. Nanotechnol. 2 (9) (2007) 577–583.
[65] Y. Song, K. Qu, C. Zhao, J. Ren, X. Qu, Graphene oxide: intrinsic peroxidase catalytic activity and its application to glucose detection, Adv. Mater. 22 (19) (2010) 2206–2210.
[66] D. Wen, W. Liu, A.K. Herrmann, D. Haubold, M. Holzschuh, F. Simon, A. Eychmüller, Simple and sensitive colorimetric detection of dopamine based on assembly of cyclodextrin-modified Au nanoparticles, Small 12 (18) (2016) 2439–2442.
[67] P.S. Teo, P. Rameshkumar, A. Pandikumar, Z.-T. Jiang, M. Altarawneh, N.M. Huang, Colorimetric and visual dopamine assay based on the use of gold nanorods, Microchim. Acta 184 (10) (2017) 4125–4132.
[68] S. Rostami, A. Mehdinia, A. Jabbari, E. Kowsari, R. Niroumand, T.J. Booth, Colorimetric sensing of dopamine using hexagonal silver nanoparticles decorated by task-specific pyridinum based ionic liquid, Sensor Actuat B: Chem 271 (2018) 64–72.
[69] S. Dutta, C. Ray, S. Mallick, S. Sarkar, R. Sahoo, Y. Negishi, T. Pal, A gel-based approach to design hierarchical CuS decorated reduced graphene oxide nanosheets for enhanced peroxidase-like activity leading to colorimetric detection of dopamine, J. Phys. Chem. C 119 (41) (2015) 23790–23800.
[70] M. Hosseini, M. Aghazadeh, M. Reza Ganjali, A facile one-pot synthesis of cobalt-doped magnetite/graphene nanocomposite as peroxidase mimetics in dopamine detection, New J. Chem. 41 (21) (2017) 12678–12684.
[71] M. Ivanova, E.D. Grayfer, E.E. Plotnikova, L.S. Kibis, G. Darabdhara, P.K. Boruah, M.R. Das, V.E. Fedorov, Pt-Decorated boron nitride nanosheets as artificial nanozymes for detection of dopamine, ACS Appl. Mater. Interfaces 11 (25) (2019) 22102–22112.
[72] Z. Yang, Y. Zhu, M. Chi, C. Wang, Y. Wei, X. Lu, Fabrication of cobalt ferrite/cobalt sulfide hybrid nanotubes with enhanced peroxidase-like activity for colorimetric detection of dopamine, J. Colloid Interface Sci. 511 (2018) 383–391.
[73] Y. Zhuang, X. Zhang, Q. Chen, S. Li, H. Cao, Y. Huang, Co_3O_4/CuO hollow nanocage hybrids with high oxidase-like activity for biosensing of dopamine, Mater. Sci. Eng. C 94 (2019) 858–866.
[74] M.X. Guo, Y.F. Li, Cu (II)-based metal-organic xerogels as a novel nanozyme for colorimetric detection of dopamine, Spectrochim. Acta A 207 (2019) 236–241.
[75] Z. Yang, F. Ma, Y. Zhu, S. Chen, C. Wang, X. Lu, A facile synthesis of $CuFe_2O_4$/Cu_9S_8/PPy ternary nanotubes as peroxidase mimics for the sensitive colorimetric detection of H_2O_2 and dopamine, Dalton Trans. 46 (34) (2017) 11171–11179.
[76] J. Zhu, X. Peng, W. Nie, Y. Wang, J. Gao, W. Wen, J.N. Selvaraj, X. Zhang, S. Wang, Hollow copper sulfide nanocubes as multifunctional nanozymes for colorimetric detection of dopamine and electrochemical detection of glucose, Biosens. Bioelectron. 141 (2019) 111450–111457.
[77] Y. Wu, P. Deng, Y. Tian, Z. Ding, G. Li, J. Liu, Z. Zuberi, Q. He, Rapid recognition and determination of tryptophan by carbon nanotubes and molecularly imprinted polymer-modified glassy carbon electrode, Bioelectrochemistry 131 (2020) 107393–107400.